Production mechanism of backward energetic protons studied from two-particle correlations in 800 MeV proton-nucleus collisions

Y. Miake,* H. Hamagaki, S. Kadota, S. Nagamiya,* S. Schnetzer,† Y. Shida, H. Steiner,‡ and I. Tanihata
Institute for Nuclear Study, University of Tokyo, Midori-cho, Tanashi-shi, Tokyo 188, Japan
and Nuclear Science Division, Lawrence Berkeley Laboratory, University of California, Berkeley, California 94720
(Received 10 September 1984)

The relative importance of various mechanisms which may play a role in the production of backward energetic protons has been studied in 800 MeV proton-nucleus collisions. Energetic protons ($P \geq 350$ MeV/c) at $\theta = 118°$ were measured in coincidence with particles emitted in the angular range from 15° to 100°. Both in-plane ($\Delta\phi = 180°$) and out-of-plane ($\Delta\phi = 90°$) coincidences were measured. The data have been decomposed into several categories depending on the excitation energy of the residual nucleus. Momentum spectra, angular distributions, and target mass dependences of these categories have been studied. The scattering of the incident proton by a correlated nucleon cluster seems to play an important role. From the proton spectrum associated with the p-d quasi-elastic scatterings, the momentum spread of the pn system ("d") inside the nucleus has been determined. The momentum spread of the "d" obtained by the p-d quasi-elastic scatterings is found to be smaller than the spread observed in heavy-ion projectile fragmentation into deuterons. From the mass dependence of the ratio of the p-d to p-p quasi-elastic scattering cross sections, the mean free path of deuterons inside the nucleus has been determined.

I. INTRODUCTION

The study of energetic proton-nucleus interactions may reveal effects of correlated nucleons in nuclear matter. In the present experiment we have measured two-particle coincidence spectra under both in-plane and out-of-plane coincidence conditions when 800 MeV protons collided with various nuclear targets. Coincidence events between p (backward) and p (forward) as well as p (backward) and d (forward) were measured over the kinematic domain shown by the hatched rectangle in Fig. 1. By focusing on specific kinematical conditions we have obtained quantitative information about various production mechanisms. Proton-deuteron quasi-elastic scattering at large momentum transfer has also been measured. From these results we have deduced the width of the momentum distribution of the pn system inside the nucleus as well as the mean free path of deuterons in nuclear matter.

Frankel *et al.* measured the inclusive spectra of backward protons and other light particles from 600–800 MeV proton-nucleus collisions.[1] Energetic protons far beyond the Fermi energy were observed. Soon after the data were presented, Amado and Woloshyn analyzed backward energetic protons in terms of single nucleon-nucleon scattering.[2] They assumed that the backward emission of nucleons, which is forbidden in free nucleon-nucleon scattering, is due to the internal motion of nucleons inside a nucleus. However, it was immediately apparent that single nucleon-nucleon scattering with a conventional internal momentum distribution (Gaussian-type) gives a cross section which is several orders of magnitude smaller than the observed one. In other words, to fit the observed spectrum a high-momentum tail of the momentum distribution is required.

In the framework of the single-scattering model, Frank-

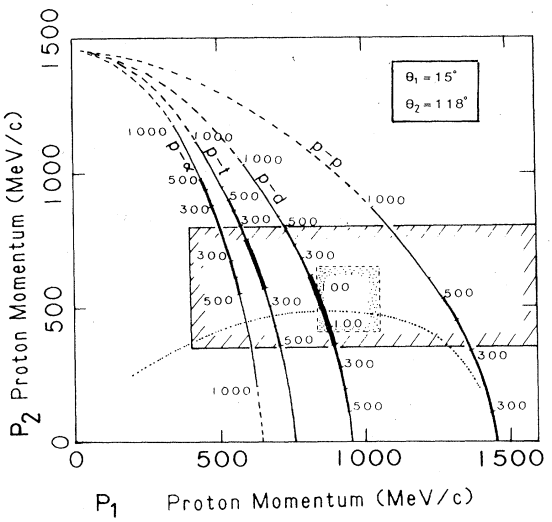

FIG. 1. The momentum region covered by the present experiment is shown by a hatched rectangle. The horizontal axis is the momentum of the forward proton at $\theta = 15°$ and the vertical axis is the momentum of the backward proton at $\theta = 118°$. Solid lines show kinematical relations between forward and backward protons produced by the elastic scattering of the incident proton with protons and nucleons clusters which have Fermi motion inside the target nucleus. Numbers beside the curves indicate the momentum of the proton (or clusters) inside the target nucleus in MeV/c. Because the breakup of clusters contributes to the two-proton coincidence measurement, curves for p-d, p-t, and p-α are drawn as a function of the internal momentum per nucleon. These curves are the kinematical loci of gentle (small relative momentum) breakup reactions. The kinematical locus of large relative momentum breakup of the p-(2N) reaction with no Fermi motion is also shown (dotted curve). The dotted rectangle shows the momentum range covered by the measurement in Refs. 20 and 21.

el *et al.* introduced the concept of quasi-two-body scaling.[3–9] They were able to reproduce the observed proton spectrum when they used an exponential-type momentum distribution, $\exp(-k/k_0)$ with $k_0 \approx 90$ MeV/c. An interpretation of the scaling based on an optical approximation is discussed by Gurvitz.[10]

A correlated-cluster model proposed by Fujita *et al.*[11–14] and a model based on the cumulative effect proposed by Baldin *et al.*[15] are also successful in explaining the inclusive spectra of backward protons. These models are based on the idea that a large momentum can be transferred to the proton when it scatters from a heavier object such as a two- or three-nucleon cluster inside the target nucleus.

Still another approach is the statistical model.[16] Knoll showed that the proton spectra were reproduced by a statistical model in which backward protons are emitted from a statistically equilibrated nucleon system. To explain the high energy tail of the backward proton distribution he concluded that four target nucleons contribute to the reaction on average.

Although the models proposed so far, namely the single-scattering model, the correlated-cluster model, and the statistical model, rely on seemingly different basic assumptions, they have had comparable success in explaining the dominant features of the observed spectra.

Two types of measurements are expected to clarify this situation: an analyzing power measurement and a two-particle correlation measurement. Frankel and Woloshyn[17] proposed that an experiment with polarized protons would be useful to distinguish the different models. They argued that only the single-scattering model gives a large analyzing power, while the correlated-cluster model and the statistical model give small or no asymmetry. The measurement was done by Frankel *et al.*[18] using a polarized 800 MeV proton beam. The analyzing power of protons emitted at around 100° is generally small, although it depends slightly on the target mass and on the momentum of the backward proton. However, since the analyzing power is very sensitive to final state interactions as well as to the details of the initial and final state wave functions, no definitive statements about the production mechanism could be made. Frankel *et al.*[22] also measured two-proton correlations in p + ^{6}Li reactions at proton energies of 600 and 800 MeV. They observed quasi-elastic scatterings of protons from ^{6}Li as well as the coincidence events between forward and backward protons corresponding to p-(2N) scattering kinematics. However, since their energy and angular ranges were restricted, the relative importance of the various production mechanisms was not discussed.

Komarov *et al.* measured two-proton correlations at a beam energy of 640 MeV.[19–21] They used a ΔE-E counter telescope to detect backward protons in the momentum range from 310 to 530 MeV/c. A range counter telescope was used for the detection of forward particles in the momentum range from 730 to 850 MeV/c. When a proton is emitted in a process involving the scattering of an incident proton on a deuteron inside the nucleus, the scattered deuteron comes out either in the form of a deuteron or two nucleons (p and n). The range of energies of the forward protons in Komarov's experiment was very limited. It included only those protons which are emitted when deuterons break up with small relative momentum between proton and neutron. Two-nucleon clusters such as p-p, n-n, or p-n singlet may also exist inside the nucleus. Thus, the idea was expanded to the more general case of p-(2N) scattering, where (2N) symbolically indicates two-nucleon clusters. They concluded that the scattering of the incident proton by cluster is the main mechanism of backward proton production.

There are characteristic two-particle correlations for each of the above three mechanisms which can be used in coincidence experiments to learn more about their role in backward proton emission. In p-p coincidences, if two protons satisfy the condition of $E_B + E_F \approx E_{\text{beam}} + m_p$, then these two protons are mainly from a p-p quasi-elastic scattering between the projectile and a proton inside the target nucleus. Here the subscripts B and F refer to backward and forward, respectively; E indicates the energy of the particle; and m_p is the proton mass. Similarly, in p-d coincidences the condition $E_B + E_F \approx E_{\text{beam}} + m_d$ selects p-d quasi-elastic scatterings.

In-plane and out-of-plane events correspond to the azimuthal separations $\Delta\phi$ between the two detected particles of 180° and 90°, respectively. In the statistical model, which implicitly assumes that each particle experiences incoherent multiple nucleon-nucleon collisions, azimuthal symmetry is expected. Any residual asymmetry due to the overall momentum conservation is expected to be small when the number of particles in the system is larger than 4.[16]

In a proton-cluster collision, clusters may break up into nucleons. These reactions are characterized by the fact that $E_B + E_F \neq E_{\text{beam}} + m_p$. The kinematical separation of these processes is illustrated in Fig. 1 together with the kinematical region covered by the present experiment.

The previous attempts of measuring two-particle coincidences by Komarov *et al.*[21] and by Frankel *et al.*[22] did not cover a kinematic domain wide enough to establish the relative importance of the various mechanisms discussed in the preceding paragraphs. Recently a coincidence experiment which covers a wider kinematical range was reported for 300 MeV incident protons.[23] Contributions from quasi-elastic scatterings as well as multiple scatterings were observed, but again no unambiguous conclusions about these mechanisms emerged.

II. EXPERIMENTAL ARRANGEMENTS AND PROCEDURES

A. General

The spectra of backward protons in coincidence with forward going particles were measured in 800 MeV proton nucleus collisions. Backscattered protons in the momentum range 330–700 MeV/c were detected at scattering angles from 103° to 153°, and forward protons and deuterons in the momentum range 480–2000 MeV/c were detected at scattering angles 15, 20, 30, 40, 55, 70, 90, and 100 deg. Although we have measured coincidence spectra at various angles, the emphasis in this paper will be on the

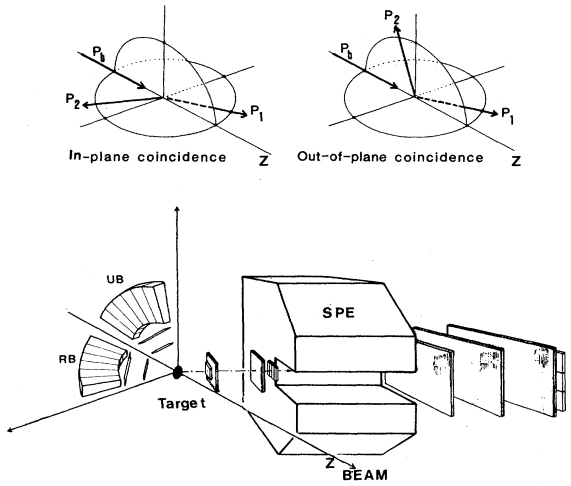

FIG. 2. Schematic view of the counter setup. Two sets of ΔE-E counters (RB and UB) covered $\theta=105°-155°$ at $\phi=90°$ and 180°. The magnetic spectrometer covered 8° in θ at $\phi=0°$ and was rotated from 15° to 100° in θ.

coincidence data where one proton is emitted at 118° and the other at 15°, because this angular combination includes both the p-p and p-(2N) scattering kinematics as shown in Fig. 1.

A magnetic spectrometer was used to detect forward particles. The spectrometer, which has an angular acceptance of $\Delta\theta=8°$, was rotated from 15° to 100°. Two sets of ΔE-E telescopes were used to detect backward protons. One telescope was in the same reaction plane as the spectrometer, while the other was perpendicular to the reaction plane. The counter setup as well as the coordinate definition is illustrated in Fig. 2. Performance of the detectors is summarized in Table I.

B. Beam and targets

We used an 800 MeV proton beam accelerated by the Bevatron at Lawrence Berkeley Laboratory. Typically the beam intensity was 10^7 to 10^8 particles per pulse and the beam repetition period was 6 s. The duration of each beam was about 600 ms.

Disks of C, NaF, KCl, Ag, and Pb 5 cm in diameter were used as targets. The typical thickness was about 0.5 g/cm^2.

The beam intensity was monitored by an ionization chamber (IC) inserted in the beam line 1.5 m upstream of the target. The IC was filled with a mixed gas of 80% Ar and 20% CO_2 at 1.05 atm. The total charge collected in the IC was measured for every beam pulse. The background charge of the IC was measured during the beam-off period. For the calibration of the IC, we placed two thin plastic scintillation counters in the beam, and measured the charge collected in the IC against the coincidence counts between these two counters at low beam intensity (10^3–10^6 particles). At higher beam intensity we used a monitor counter telescope (MC) which counted scattered particles from a target. Then the counting rate of the MC was compared with the charge of the IC. The linearity between the collected charge in the IC and the counts in the MC was good within a few percent over the whole intensity range used in the experiment.

TABLE I. Performance of the detectors.

	Magnetic spectrometer	ΔE-E telescope
Particles	π,p,d,t,^{3}He	π,p,d
Momentum range (MeV/c)	480–2000	330–700
Momentum resolution (typical)	7%	9%
Solid angle (msr)	12	29×5
Covered angle	15°–100° ($\Delta\vartheta=8°$)	105°–155°

C. The ΔE-E counters

Backward-emitted particles were detected by plastic scintillation ΔE-E counter telescopes. Two sets of telescopes covered an angular range of $\theta=105°-155°$, one at $\phi=180°$ (RB) and the other at $\phi=90°$ (UB). Figure 3 shows a plan view of the telescope RB. The first counter (RB1) and the second counter (RB2) measured the energy loss (dE/dx) of a particle. Since RB2 had phototubes on both ends of the plastic scintillator, the hit position could also be determined. The third counter (RB3) consisted of five energy (E) counters RB3a, RB3b, RB3c, RB3d, and RB3e and a veto counter RB3f. Each of these E counters covered $\Delta\theta=\pm5°$. The veto counter RB3f was used to reduce the background from stray beam particles.

A typical scatter plot of the pulse heights in the ΔE and

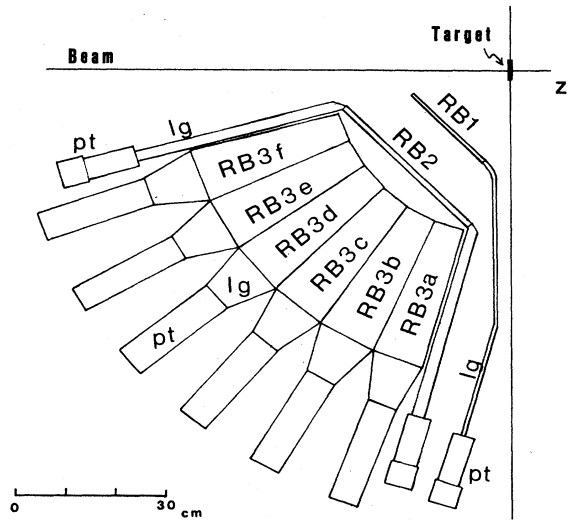

FIG. 3. Plan view of the ΔE-E counter, lg; Lucite light guides, pt; photomultiplier tubes. All the counters are made of plastic scintillators.

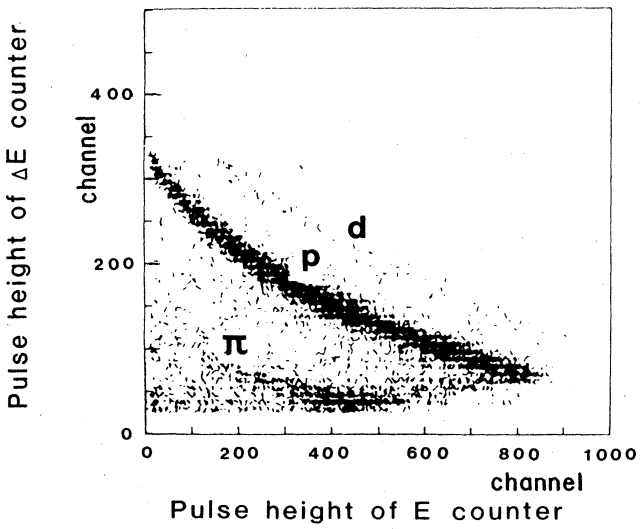

FIG. 4. A typical scatter plot of E vs ΔE. Clear separations between the pion, proton, and deuteron are seen.

E counters is shown in Fig. 4. A clear separation of protons, deuterons, and pions is seen in the figure. The maximum proton momentum measured by the telescope was 700 MeV/c which was determined by the total thickness of the telescopes. The minimum proton momentum was 330 MeV/c. The probability of secondary reactions in the E counter was estimated to be about 32% for a 700 MeV/c proton. The detection efficiency was not affected by the secondary reactions, but the pulse height was reduced and thus affected the energy resolution.

For energy calibration we set the telescope behind a time of flight (TOF) counter with a flight path of 2 m. The velocity of a particle was measured by the TOF

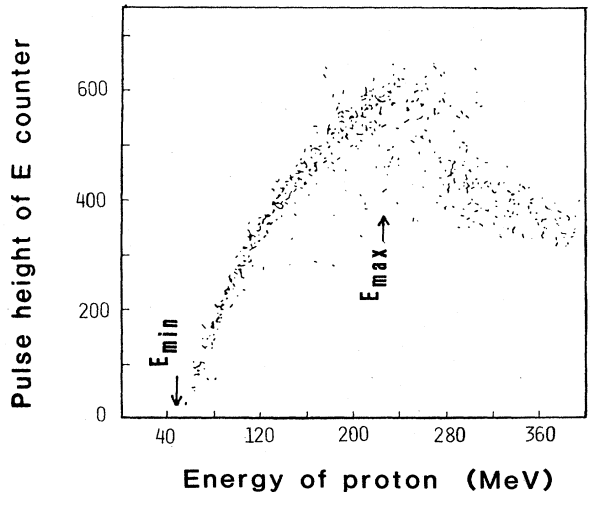

FIG. 5. Energy calibration curve of a ΔE-E counter. The calibration was done by the TOF counter. The energy E_{min} and E_{max} written in the figure indicate the minimum and the maximum energies of the ΔE-E counter calculated by the range-energy relation.

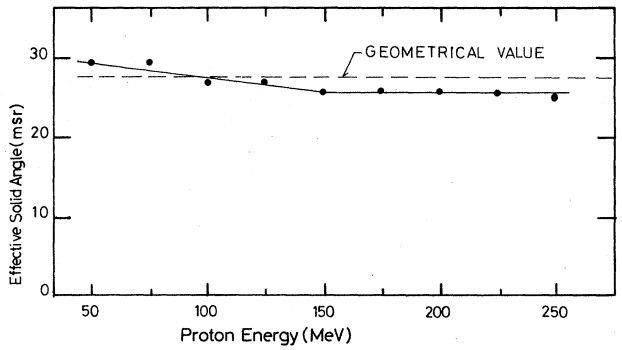

FIG. 6. The effective solid angle of the E counters as a function of the proton momentum. The change of the solid angle is due to multiple scattering in the first and second scintillators. The solid line in the figure shows the solid angle used for the present analysis. A dashed line shows the geometrical solid angle.

counter, whereas the dE/dx and the energy were measured by the ΔE-E counter. Particle identification was made with the ΔE-E counter and the energy was determined from the proton velocity as measured by the TOF counter. Figure 5 shows the result of the calibration. The E_{min} and the E_{max} written in Fig. 5 indicate the minimum and the maximum proton energies in the ΔE-E counter calculated using the range-energy relations. To understand the nonlinearity between the energy and the pulse height, the position dependence of the light collection efficiency was measured using cosmic rays. The data showed that the light collection efficiency was smaller when the source of light was farther from the entering surface, namely, in the stopping region of high energy particles. The intrinsic momentum resolution was 9% at a proton momentum of 480 MeV/c and 8.5% at 700 MeV/c. In the actual experiment, however, the finite thicknesses of the targets worsen the resolutions to 12% at 480 MeV/c and 10% at 700 MeV/c.

The effective solid angle of the telescope was estimated by a Monte Carlo calculation which includes multiple Coulomb scattering. Because the first and second counters (RB1 and RB2) subtended wider solid angles than the E counter, low energy protons could be kicked into the E counter by multiple scattering. Therefore the effective size of the E counter is slightly larger than the geometrical size. On the other hand, high energy protons escape from the side of the E counter, which reduces the effective size. The effective solid angle as a function of proton energy is shown in Fig. 6.

TABLE II. Momentum resolution of the magnetic spectrometer.

Momentum P (MeV/c)	Resolution $\Delta P/P$ (%)
500	9.0
750	6.0
1000	8.5
1250	11.0

D. The magnetic spectrometer

Forward emitted particles were detected by a magnetic spectrometer. The spectrometer was set at $\phi=0°$ and rotated from $\theta=15°$ to 100°. The magnetic spectrometer consisted of a C magnet, a scintillation counter telescope, and multiwire proportional chambers (MWPC's). The bending angle in the magnetic field, the time of flight, and the pulse height of the plastic scintillation counters were measured in order to identify the particle and to determine its momentum. The momentum resolution of the spectrometer was governed by the wire spacing of the MWPC's for high energy particles and by multiple Coulomb scattering in the plastic scintillation counters for low energy particles. The momentum resolution is listed in Table II.

The magnetic spectrometer used in the present experiment is the same one as described in Ref. 24. A more detailed description of the spectrometer is given there.

E. Electronics and data acquisition system

We used two types of event triggers,

$$\text{INCL}=\text{SPE}+\text{RB}+\text{UB}\,, \tag{2.1}$$

$$\text{COIN}=\text{SPE}^*(\text{RB}+\text{UB})\,, \tag{2.2}$$

where the asterisk means logical AND and the plus sign means logical OR. The symbols SPE, RB, and UB indicate the signals from the magnetic spectrometer and the ΔE-E telescopes RB and UB, respectively. The trigger INCL refers to the single-particle inclusive measurement and COIN to the two-particle coincidence measurement. A SPE*RB coincidence signals the in-plane emission ($\Delta\phi=180°$) of two particles whereas SPE*UB is the analogous out-of-plane emission ($\Delta\phi=90°$) signal.

We monitored the accidental coincidence rate of each telescope by shifting the timing by about 200 ns. The accidental coincidences were typically 2% of the real coincidence rates. Even though these accidental coincidences were accepted as trigger events, most of these events were later rejected for failing consistency checks in the off-line analysis. The fraction of accidental coincidences between two different detectors (SPE*RB and SPE*UB) were calculated from the coincidence resolving time (30 ns) and the microscopic duty factor of the beam. The admixture of accidental two-particle coincidences was estimated to be less than 5%.

For on-line data taking we used an MBD-11 (microprogrammable branch driver) which was connected to a PDP-11/20 computer. On-line data analysis was performed between beam bursts. Histograms and scatter plots of any desired combinations of the analog-to-digital converter (ADC), time-to-digital converter (TDC), wire-chamber hit patterns, and bending angle distribution were displayed during the run in order to check that the system was working properly. Off-line data analysis was done by a VAX-11/780 at the Bevalac and by a FACOM M 180-II-AD at the Institute for Nuclear Study of University of Tokyo.

TABLE III. Conditions of the measurements.

Inclusive cross section of the proton ($p + A \rightarrow p + X$) ϑ: 108°, 118°, 128°, 138°, 148° p: 330—700 MeV/c
Two particle coincidence
p-p coincidence ($p + A \rightarrow p + p + X$) and p-d coincidence ($p + A \rightarrow p + d + X$)
ϑ_1 (p or d): 15°, 20°, 30°, 40°, 55°, 70°, 90°, 100° P_1 (p or d): 480—2000 MeV/c
ϑ_2 (p): 118° P_2 (p): 330—700 MeV/c
$\Delta\varphi=\varphi_1-\varphi_2$: 180° (in plane) and 90° (out of plane)

III. EXPERIMENTAL RESULTS

The in-plane and out-of-plane coincidence cross sections associated with backward protons as well as the inclusive cross sections of backward protons were measured. Conditions of these measurements are tabulated in Table III. In this paper we present only those data which provide most of the essential physics information relating to the goals of this experiment. The cross sections for the other cases that are not shown in this report may be obtained directly from the authors.

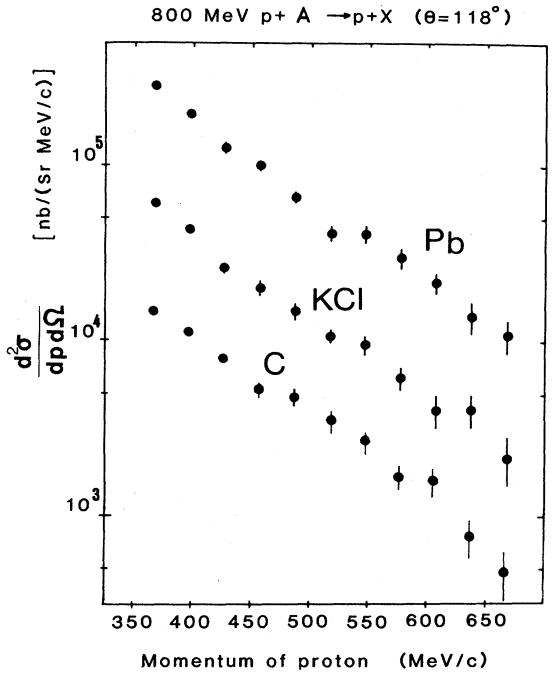

FIG. 7. Inclusive momentum spectra of protons at $\theta=118°$ in 800 MeV p + Pb, p + KCl, and p + C collisions. Error bars in the figure show the statistical errors. The systematic error is estimated to be less than 20%.

A. Inclusive spectra of backward protons

Figure 7 shows examples of proton inclusive momentum spectra at $\theta=118°$ with C, KCl, and Pb targets at an incident proton energy of 800 MeV. The error bars in the figure show only statistical errors. The systematic error of the absolute cross section was estimated to be less than 20%. The spectra can be parametrized by

$$\frac{d^2\sigma}{dP\,d\Omega}=C_0 e^{(-P/P_0)}, \tag{3.1}$$

with the slope parameters P_0,

$$P_0=94\pm6 \text{ MeV}/c \text{ for C}, \tag{3.2}$$

$$P_0=87\pm4 \text{ MeV}/c \text{ for KCL}, \tag{3.3}$$

and

$$P_0=85\pm4 \text{ MeV}/c \text{ for Pb}. \tag{3.4}$$

These values of the slope parameter are consistent with previous data in Refs. 1–6.

In Fig. 8 the momentum integrated cross sections, $d\sigma(\theta)/d\Omega$, are plotted as a function of the emission angle. Integration was done over the momentum range from 350 to 700 MeV/c. Each datum point covers $\pm5°$ in θ. Again, protons from C, KCl, and Pb show a similar behavior. In Fig. 9 $d\sigma(\theta)/d\Omega$ at $\theta=118°$ is plotted as a function of the target mass number A. It can be parametrized by,

$$d\sigma(118°)/d\Omega=0.19A^{1.0} \text{ (mb/sr)}. \tag{3.5}$$

The power dependence is found to be constant within the present angular range (180°–148°). It is larger than that of the total reaction cross sections ($\sim A^{2/3}$) and is consistent with previous data.[17,21]

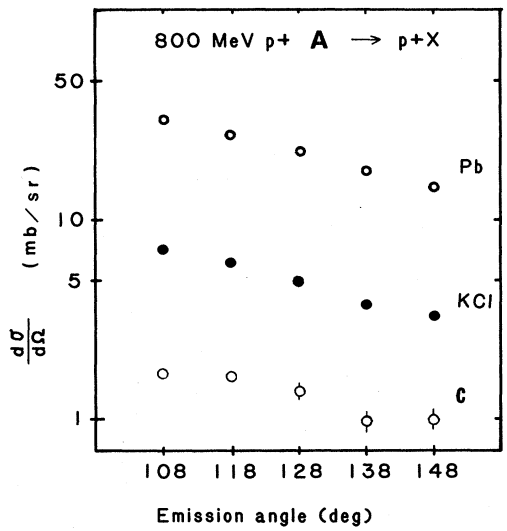

FIG. 8. Angular distributions of the inclusive protons. The cross sections are obtained by integration over the momentum range from 350 to 700 MeV/c. Statistical errors are smaller than the size of the plotted circles unless indicated. The systematic error is estimated to be less than 20%.

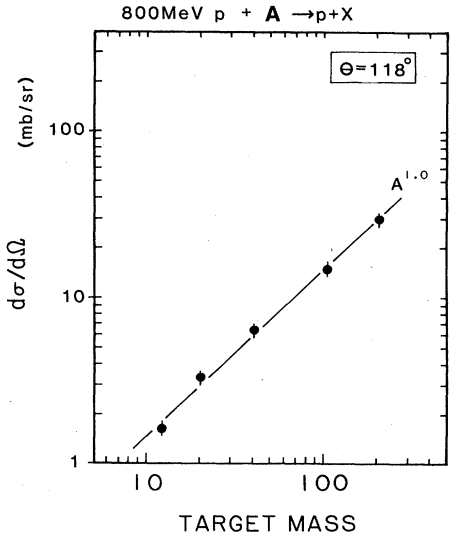

FIG. 9. Target mass dependence of the inclusive proton cross section. Error bars show only statistical errors.

B. Momentum-momentum correlations

Figure 10 shows momentum-momentum (P_1 vs P_2) scatter plots for in-plane (a) and out-of-plane (b) events when one of two protons is detected at $\theta_1=15°$ and the other at $\theta_2=118°$ in p + KCl collisions. The size of the circle in the figure indicates the number of events accumulated for each

$$\Delta P_1\times\Delta P_2=60 \text{ MeV}/c\times20 \text{ MeV}/c$$

bin. The solid curve in Fig. 10 shows the kinematical locus of p-p quasi-elastic scatterings. In drawing the curve we assumed 30 MeV binding energy for a proton inside the target nucleus. Numbers along the curve indicate the momenta of the protons (in MeV/c) inside the nucleus. We see a concentration of the events along the bottom part of the curve. As can be seen from the values of the internal momenta, these events are consistent with quasi-elastic proton scatterings from protons with large internal momenta ($P_F\geq300$ MeV/c).

The dashed line in Fig. 10 shows the kinematical locus of p-d quasi-elastic scatterings followed by deuteron breakup into a proton and a neutron with zero relative momentum. We assumed the binding energy with which deuterons are bound to the nucleus to be 60 MeV. This value is the one obtained from a fit to the p-d quasi-elastic scattering spectra (see Sec. IV C 1). The numbers beside the line indicate the momenta of deuterons inside the nucleus. The dotted curve in the figure shows the kinematical locus of protons from the breakup of stationary deuterons with finite relative momentum between the proton and neutron of the final state. The crossing point between the dashed and dotted lines indicates the kinematical point where a deuteron with zero internal momentum breaks up into a proton and a neutron with zero relative momentum. A broad distribution of events is seen in both the in-plane and out-of-plane cases. The out-of-plane

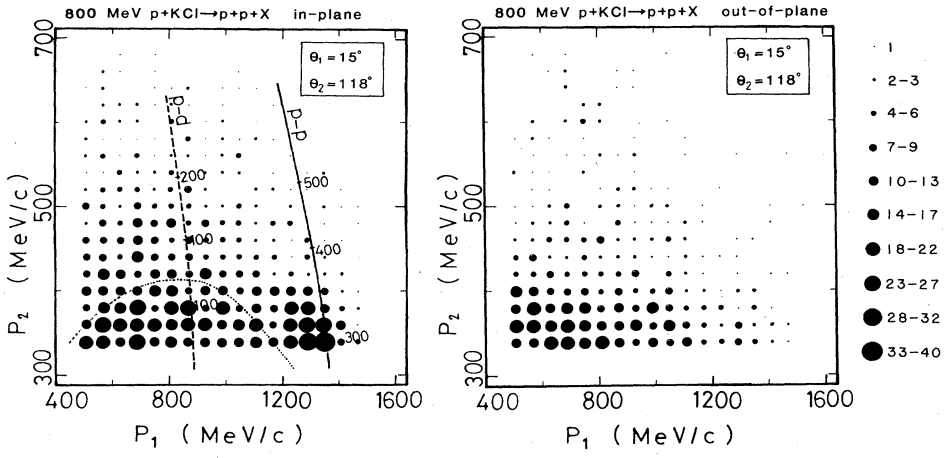

FIG. 10. Momentum-momentum scatter plots of two protons for in-plane coincidence events (a) and for out-of-plane coincidence events (b). One unit in the figure corresponds to 2.07 nb/(sr MeV/c)^2. See the text for further information.

coincidence events tend to concentrate in the low-momentum region.

Figure 11 shows in-plane (a) and out-of-plane (b) momentum-momentum scatter plots between forward deuterons ($\theta_d = 15°$) and backward protons ($\theta_p = 118°$) in p + KCl collisions. The peak near the kinematics corresponding to p-d elastic scattering, which is shown by "+" in the figure, indicates the existence of p-d quasi-elastic scatterings.

C. A classification of the events

In p-p coincidence events, we used the excitation energy (W) of the residual nuclear system, which contains ($A-1$) nucleons and possibly pions, as a parameter to classify the reaction mechanism. The reaction under discussion is

$$p_i + A \rightarrow p_1 + p_2 + (A-1) , \tag{3.6}$$

where p_i is the incident proton, p_1 and p_2 are the detected protons, A is the target nucleus, and ($A-1$) is the residual nuclear system. Here ($A-1$) is not necessarily the ground state of the nucleus. The excitation energy (W) of the residual nuclear system is defined by,

$$W = (E_{A-1}^2 - P_{A-1}^2)^{1/2} - E_{\text{g.s. of } A-1} , \tag{3.7}$$

where E_{A-1} and P_{A-1} are given by,

$$E_{A-1} = E_i + E_A - E_1 - E_2 \tag{3.8}$$

and

$$\mathbf{P}_{A-1} = \mathbf{P}_i - \mathbf{P}_1 - \mathbf{P}_2 , \tag{3.9}$$

where E_j is the total energy and $\mathbf{P}_j$ momentum of particles $j = i$, 1, 2, $A-1$, or A.

The number of events as a function of W is plotted in Fig. 12. Solid circles in this figure represent the in-plane coincidence events and open circles the out-of-plane coincidence events. A difference between the in-plane coincidence and the out-of-plane coincidence rate is clearly seen in Fig. 12. The out-of-plane coincidence events increase monotonically with W, but the in-plane coincidences show a peak near $W = 0$ which corresponds to the p-p quasi-elastic scattering (QES) events. Because p-p QES tends to cause two-proton emission in the same reaction plane, it is reasonable that the yield at $W \approx 0$ should

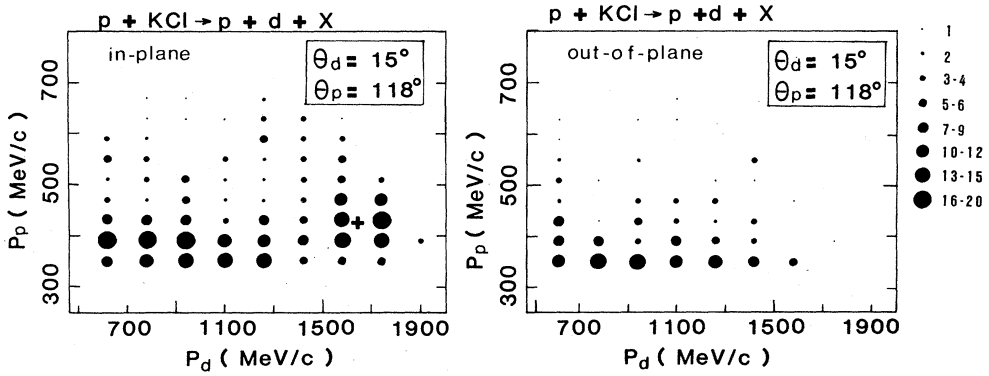

FIG. 11. Momentum-momentum scatter plots of proton-deuteron coincidence events. The symbol "+" shows the kinematics of the p-d elastic scattering.

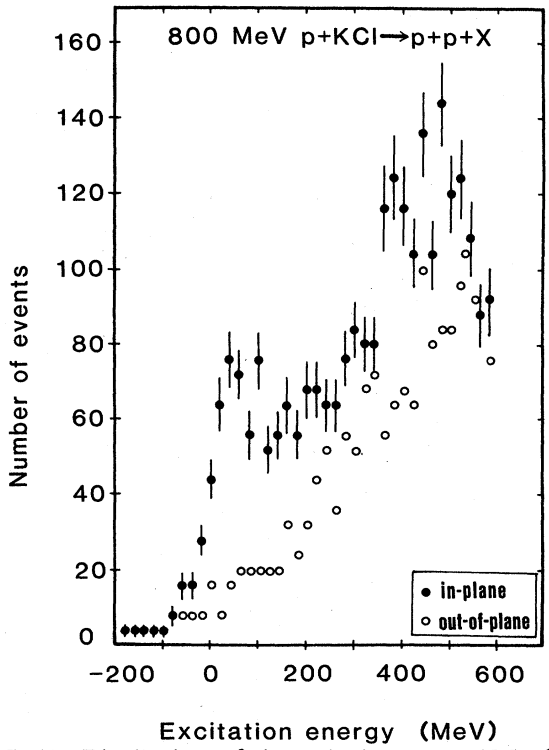

FIG. 12. Distributions of the excitation energy (W) of the residual nucleus for p-p events. Statistical errors are not shown for the out-of-plane data but they are similar to those for the in-plane data. The peak near $W=0$ shows the contribution from p-p quasi-elastic scatterings. Shift of the peak position from exact $W=0$ reflect the binding energy of proton. Another peak at $W\approx 450$ MeV is due to the instrumental kinematical limit.

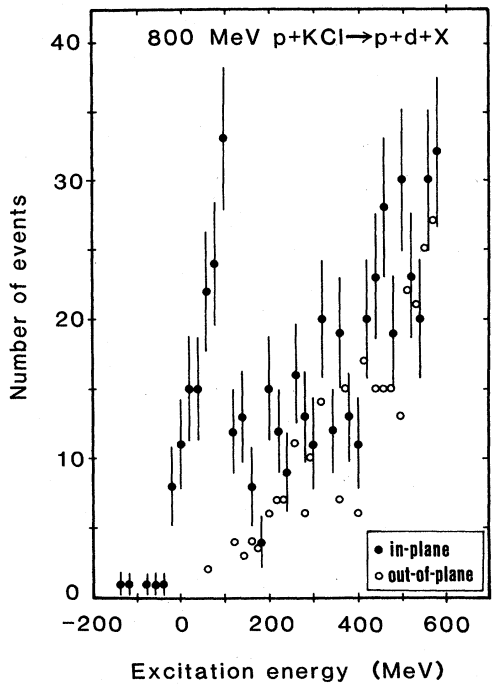

FIG. 13. Distributions of W for p-d events. The peak corresponding to p-d QES is clearly seen.

be higher for the in-plane coincidences than for the out-of-plane coincidences.

The other important feature here is the fact that the number of in-plane coincidence events is greater than that for out-of-plane coincidences by a factor of 2 in the region of $W=200$–400 MeV. If the excitation energy is shared by many nucleons, the asymmetry is expected to be small because overall momentum conservation affects the correlation only weakly when many nucleons are involved in the reaction.[16] Therefore the data suggest that the excitation energy is most likely shared by a small number of nucleons.

For use in the subsequent discussion we classify the coincidence events into three categories:

(1) "p-p QES"—in-plane coincidence events with W less than 100 MeV;

(2) "p-p non-QES"—in-plane coincidence events with W more than 100 MeV;

(3) "p-p OPC"—out-of-plane coincidence events.

Excitation spectra of the residual ($A-2$) nucleon system for the p-d coincidence events are shown in Fig. 13. A clear peak corresponding to the p-d QES is seen in the in plane coincidence events. We make a similar classification for p-d events.

(1) "p-d QES"—in-plane coincidence events with W less than 100 MeV;

(2) "p-d non-QES"—in-plane coincidence events with W more than 100 MeV;

(3) "p-d OPC"—out-of-plane coincidence events.

D. Slope factors of the backscattered protons

To see the relation of these classified events to the inclusive spectrum, the slope factors of the backward protons are listed for each case. Figure 14 shows proton spectra at 118° for the three categories of p-p coincidence events which were fitted by the functional form,

$$\frac{d^3\sigma}{d\Omega_1 d\Omega_2 dP_2}=C_0 e^{(-P_2/P_0)}. \tag{3.10}$$

The fitted values of P_0 are 55 ± 5, 91 ± 5, and 68 ± 6 MeV/c for "p-p QES," "p-p non-QES," and "p-p OPC," respectively.

Figure 15 shows the momentum spectra of the backward protons for the p-d coincidence events. The "p-d QES" spectrum shows a peak structure so that the slope factor was not obtained. On the other hand the "p-d non-QES" and the "p-d OPC" shows the exponential shape with slope factors P_0 of 94 ± 8 and 73 ± 7 MeV/c, respectively.

The slope factors for all of the categories described above for p + KCl collisions are summarized in Table IV. Also included are the data from other angular combinations as well as the slope factor of the inclusive spectrum at 118°. The slope factors are almost independent of the coincidence angle θ_1 except for "p-p non-QES," where they decrease at larger angles. A similar dependence of

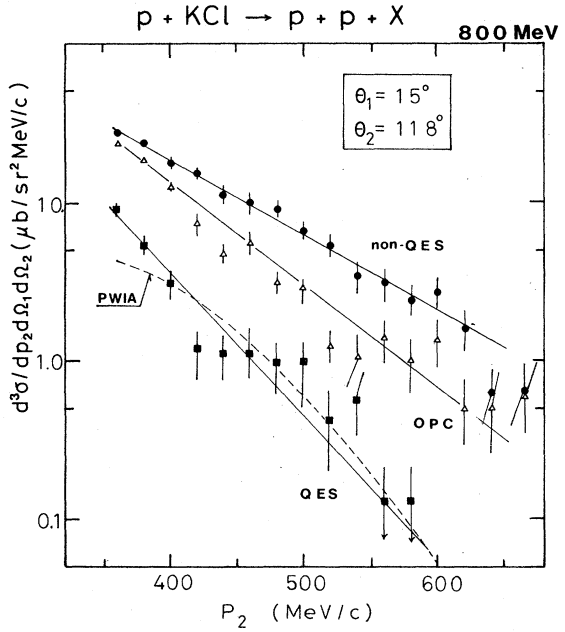

FIG. 14. Spectra of the backward protons for the different categories in p + KCl collisions. Solid lines are the exponential fit to the data. Error bars in the figure show only statistical errors. The dotted curve shows the result of PWIA calculations (see discussion in Sec. IV B).

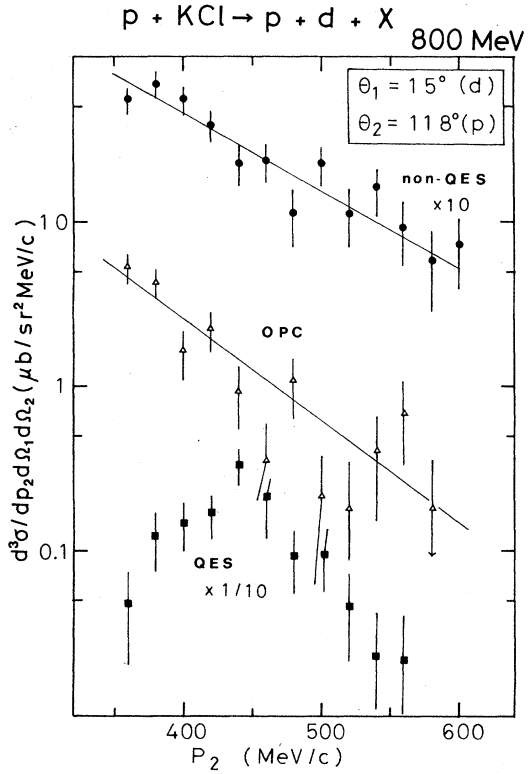

FIG. 15. Spectra of the backward protons for the different categories of p-d events. Solid lines are the exponential fit to the data. Error bars in the figure show only statistical errors.

the slope factors on the coincidence particle angle is observed for other targets. The target dependence of the slope factors is weak as shown in Table V for the data at $\theta_1 = 15°$ and $\theta_2 = 118°$.

The value of P_0 for "p-p non-QES" agrees with that observed in inclusive spectra. This fact suggests a close relationship between these two spectra. The P_0 of "p-p OPC" is slightly smaller than that of inclusive. The P_0 of "p-p QES" is considerably smaller than that of inclusive. Consequently, at high momentum "p-p QES" does not contribute appreciably to the inclusive spectrum.

E. The momentum integrated cross sections

To study the relative importance of each class of events, the two-particle cross sections were integrated over the momenta. The integration was made over the momentum range covered by the present detector system, namely $480 \leq P_1 \leq 2000$ MeV/c (forward) and $330 \leq P_2 \leq 700$ MeV/c (backward). The integrated cross sections

TABLE IV. Slope factors (P_0 in MeV/c) of backward proton spectra in p + KCl reactions [coincidence events between a backward proton at $\vartheta_2 = 118°$ and a forward particle (p or d) at various angles ϑ_1].

	Coincidence				
ϑ_1	p-p QES	p-p non-QES	p-p OPC	p-d non-QES	p-d OPC
(deg)	(MeV/c)	(MeV/c)	(MeV/c)	(MeV/c)	(MeV/c)
15	55±5	91±6	68±6	94±8	73±7
20	52±7	81±8	62±7	90±10	83±15
30		87±6	57±10	92±10	74±10
40		83±8	61±5	89±9	55±7
55		87±8	70±7		
70		70±10	53±15		
90		76±10	57±15		
100		70±9			
Inclusive at 118°					
87±2 (MeV/c)					

TABLE V. Slope factors of (P_0 in MeV/c) of backward proton spectra [coincidence events between a backward proton at $\vartheta_2=118°$ and a forward particle (p or d) at $\vartheta_1=15°$] (800 MeV p + A).

Target	C	KCl	Pb
Inclusive	88±1	87±2	85±2
p-p QES	56±4	55±3	56±4
p-p non-QES	85±5	91±5	92±4
p-p OPC	72±5	72±3	80±4
p-d QES		(non exponential shape)	
p-d non-QES	a	94±8	84±9
p-d OPC	a	73±7	77±8

[a]Present statistics are too poor to be fitted.

($d^2\sigma/d\Omega_1 d\Omega_2$) thus obtained are listed in Tables VI and VII.

The θ_1 dependences of ($d^2\sigma/d\Omega_1 d\Omega_2$) (for fixed $\theta_2=118°$) are plotted in Figs. 16 and 17 for the KCl target. It can be seen that "p-p QES" falls off rapidly with θ_1, while "p-p non-QES" and "p-p OPC" fall off more slowly. The ratio of the cross sections for "p-p non-QES" to "p-p OPC" is nearly constant over a wide range. A similar behavior is observed in the p-d coincidence data (Fig. 17).

The momentum integrated cross sections at $\theta_1=15°$ and $\theta_2=118°$ are also plotted as a function of the target mass number (A) in Figs. 18 and 19. The different categories show different A dependences. The weak A dependence ($A^{0.5}$) observed in "p-p QES" is consistent with the idea that the quasi-elastic scatterings occur at the surface of the nucleus. Slightly stronger mass dependences are observed in "p-p non-QES" ($A^{0.6}$) and in "p-p OPC" ($A^{0.76}$). The stronger mass dependence for "p-p OPC" may indicate that several particles are involved in the production mechanism. This idea is also consistent with the fact that the ratio between in-plane coincidence and out-of-plane coincidence events is smaller for heavier targets because more nucleons are likely to be involved in such collisions than in the case of a light target. The A dependence of the "p-p non-QES" ($A^{0.6}$) is stronger than the $A^{0.39}$ observed by Komarov *et al.*[21] In their experiment, a range counter telescope was used to detect the forward proton. It might be possible that this technique has weak rejection power of protons from p-p QES and thus introduced systematic effects in the determination of the A dependence.

The A dependence of the "p-d OPC" events and "p-d non-QES" increase rapidly with target mass whereas "p-d QES" shows a weaker dependence. The comparison of the A dependences of p-p and p-d events will be discussed in conjunction with the mean free path of deuterons inside the nuclei.

IV. DISCUSSION

A. Reaction mechanism in backward proton production

We discuss here the relative importance of the various reaction mechanisms in the production of backward energetic protons. We classify the coincidence events into the categories described in the previous sections. In order to estimate the contribution of each type to the inclusive spectra, we integrate the two-particle coincidence cross section ($d^2\sigma/d\Omega_1 d\Omega_2$) over θ_1. The emission angle of the backward proton is fixed at $\theta_2=118°$. In order to integrate from $\theta_1=0°$ to 180° the cross sections were extrapolated to smaller angles (from 0° to 15°) and to larger angles (from 100° to 180°). The error due to these extrapolations is estimated to be less than 20%. The integrated cross section σ_I of each reaction component for p + KCl

TABLE VI. Two-particle coincidence cross sections for 800 MeV/c p + KCl, $d^2\sigma/d\Omega_1 d\Omega_2$ at $\vartheta_2=118°$.

$\vartheta_1=$	15°	20°	30°	40°	55°	70°	90°	100°
				(mb/sr^2)				
p-p QES	0.49 ±0.03	0.26 ±0.03	0.067 ±0.012	0.010 ±0.003	0.000 ±0.002	0.000 ±0.001	0.000 ±0.001	0.000 ±0.001
p-p non-QES	2.74 ±0.08	2.36 ±0.09	1.87 ±0.06	1.09 ±0.03	0.60 ±0.03	0.28 ±0.02	0.08 ±0.01	0.040 ±0.005
p-p OPC	1.75 ±0.08	1.33 ±0.08	1.10 ±0.05	0.64 ±0.03	0.30 ±0.03	0.16 ±0.02	0.07 ±0.01	0.026 ±0.004
p-d QES	0.27 ±0.03	0.06 ±0.02	0.006 ±0.004	0.001 ±0.001	0.000 ±0.002	0.000 ±0.01	0.000 ±0.001	0.000 ±0.001
p-d non-QES	0.71 ±0.04	0.49 ±0.04	0.42 ±0.03	0.20 ±0.01	0.10 ±0.01	0.08 ±0.01	0.024 ±0.006	0.007 ±0.002
p-d OPC	0.40 ±0.03	0.21 ±0.04	0.29 ±0.03	0.15 ±0.01	0.06 ±0.01	0.032 ±0.008	0.020 ±0.006	0.006 ±0.002

TABLE VII. Two-particle coincidence cross sections for 800 MeV p + nucleus, $d^2\sigma/d\Omega_1 d\Omega_2$ at $\vartheta_1=15°$ and $\vartheta_2=118°$.

Target	C	NaF	KCl	Ag	Pb
				(mb/sr^2)	
p-p QES	0.24 ±0.02	0.21 ±0.03	0.49 ±0.03	0.62 ±0.07	0.99 ±0.13
p-p non-QES	0.98 ±0.05	1.43 ±0.07	2.74 ±0.08	4.42 ±0.19	5.10 ±0.29
p-p out of plane	0.57 ±0.04	0.95 ±0.07	1.89 ±0.08	3.55 ±0.18	4.98 ±0.32
p-d QES	0.19 ±0.03	0.18 ±0.03	0.27 ±0.03	0.22 ±0.05	0.33 ±0.09
p-d non-QES	0.23 ±0.02	0.34 ±0.03	0.71 ±0.04	1.30 ±0.10	1.18 ±0.13
p-d out of plane	0.10 ±0.02	0.20 ±0.03	0.40 ±0.03	0.70 ±0.08	1.17 ±0.16

collisions listed in Table VIII has a systematic error of about 30% in the absolute value. Relative errors are less than 20%. It can be seen that contributions from "p-p non-QES" and "p-p OPC" are the largest.

The slope factors of the backward proton spectra for the different categories of once integrated two-particle coincidence cross sections are compared in Table V. The "p-p QES" shows a smaller P_0 value than that of the inclusive spectrum. Its integrated cross section is very small. This shows again that the "p-p QES" events do not contribute significantly to the production of backward energetic protons.

As seen in Fig. 15 the cross section of "p-d QES" is almost as large as "p-d non-QES" at angles $\theta_d=15°$ and $\theta_p=118°$ in p + KCl collisions. The high momentum part of the backward proton spectrum attributed to "p-d QES" has about the same slope as the inclusive spectrum. This fact is consistent with the idea that cluster scatter-

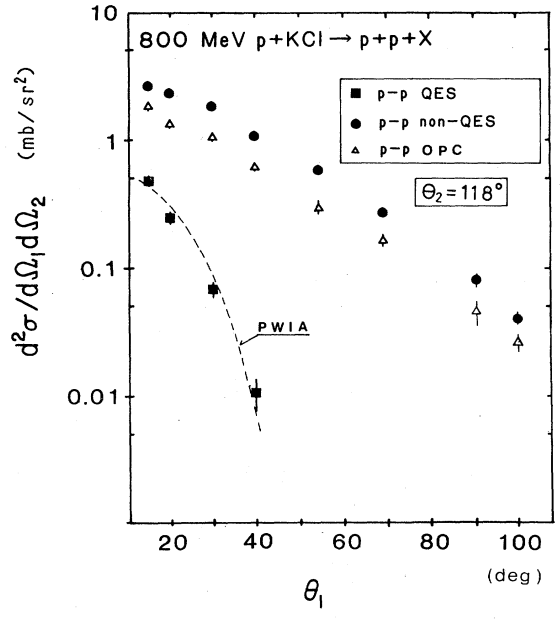

FIG. 16. Angular distributions of forward protons in coincidence with backward protons at $\theta_2=118°$. Error bars represent only statistical errors. The dotted curve shows the result of PWIA calculations (see Sec. IV B).

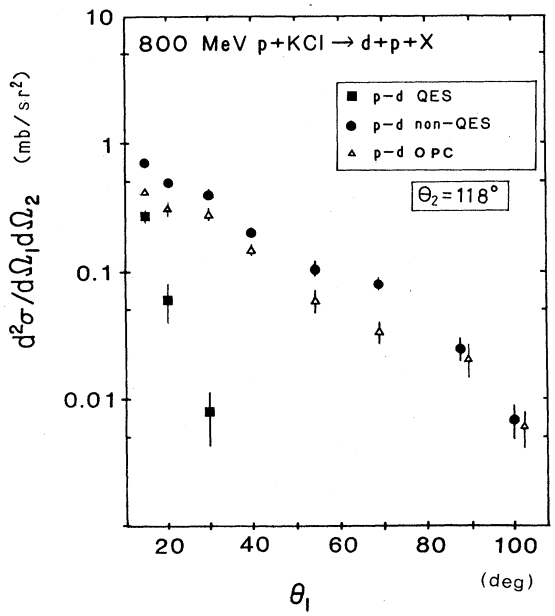

FIG. 17. Angular distributions of deuterons in coincidence with backward ($\theta=118°$) protons. Error bars indicate statistical errors only.

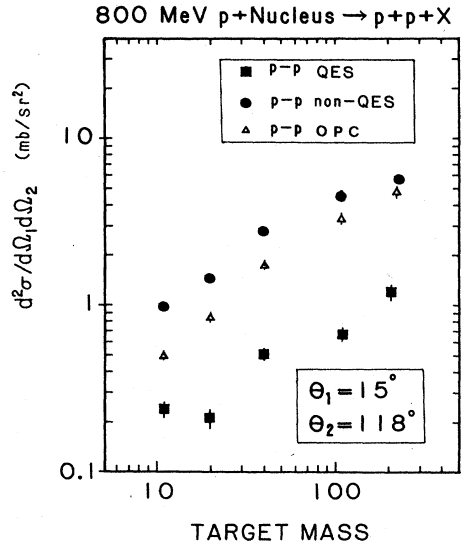

FIG. 18. Mass number dependence of the p-p coincidence cross section. Only statistical errors are shown.

ings play an important role in backward proton inclusive processes. On the other hand the integrated cross sections of "p-d QES" are relatively small compared to the other categories. The observed target mass dependence ($\approx A^{0.17}$) of "p-d QES" may be due to the fact that a deuteron produced through p-d QES is more likely to be rescattered and break up into a proton and a neutron in the heavier mass targets. The rescattering probability or the mean free path of the deuteron will be discussed later in Sec. IV C 2.

The slope factor of the "p-p non-QES" spectrum is larger than that of "p-p QES." Its value is close to that of the inclusive spectrum. This fact suggests that "p-p non-QES" contributes significantly to the inclusive production

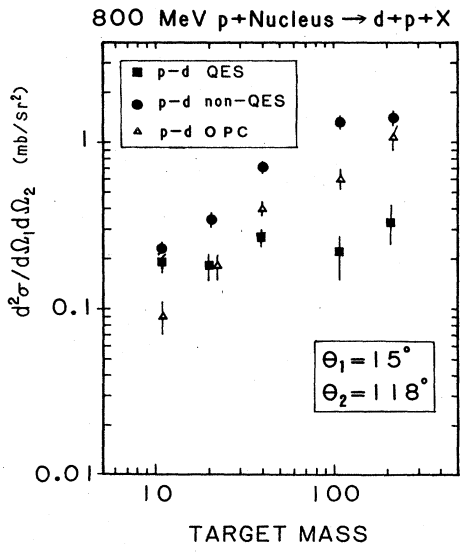

FIG. 19. Target mass number dependences of the p-d coincidence cross sections. Only statistical errors are shown.

TABLE VIII. Integrated cross sections, $\sigma_1 = \int_0^{\pi} d^2\sigma / d\Omega_1 d\Omega_2 \sin\vartheta_1 d\vartheta_1$ (800 MeV p + KCl).

	σ_1 (mb/rad sr)
p-p QES	0.05
p-p non-QES	0.80
p-p OPC	0.47
p-d QES	0.03
p-d non-QES	0.16
p-d OPC	0.11

of backward protons. This conclusion is also supported by the large cross section of this component.

The value P_0 of "p-p OPC" is slightly smaller than that of the inclusive spectrum. It is therefore unlikely that "p-p OPC" is the main component at the highest momentum. From the integrated cross section (Table VIII), however, a significant contribution from "p-p OPC" is indicated in the present momentum range.

Figure 20 shows the backward proton spectra for "p-p non-QES" minus "p-p OPC" in collisions of p + KCl as compared with the spectrum of "p-d QES." Both spectra show peaks at around 430 MeV/c. The similarity of the two distributions suggests that the basic reaction mechanism of "p-d QES" and the excess part of "p-p non-QES" may be related to each other. In Fig. 21 we also show contour lines of the cross section ($d^4\sigma/dP_1 dP_2 d\Omega_2 d\Omega_2$)

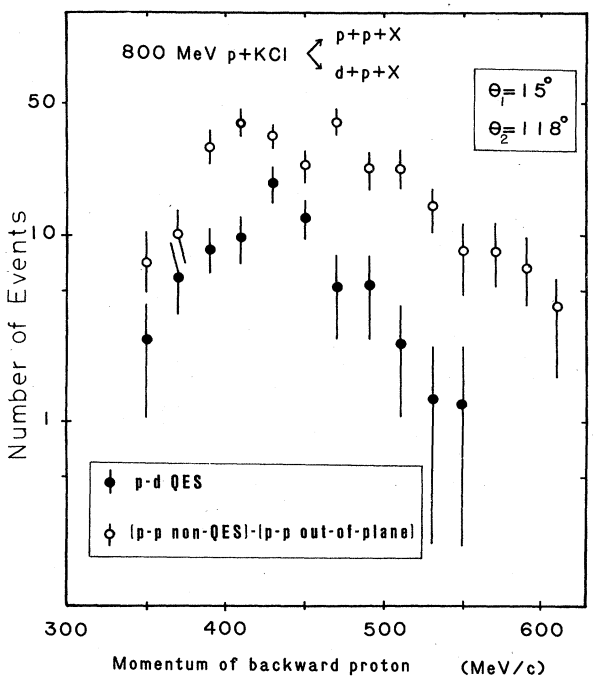

FIG. 20. Backward proton spectrum of the "p-d QES" (solid circles) events and a difference spectrum between "p-p non-QES" and "p-p OPC" in the collision of p + KCl at the angles $\theta_1(=\theta_d)=15°$ and $\theta_2=118°$. Only statistical errors are shown in the figure.

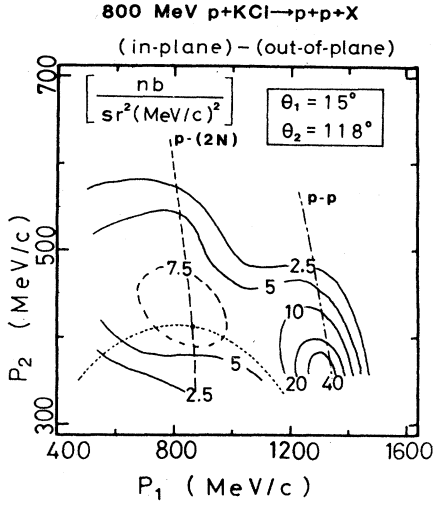

FIG. 21. Contour line plot of the difference between the double differential cross sections ("p-p in-plane"—"p-p OPC"). Kinematical loci of p-p QES and p-(2N) breakup reactions are also shown. A broad concentration of the events is seen around the p-(2N) breakup region.

for p-p in-plane coincidence events minus out-of-plane events. Kinematical loci for p-p quasi-elastic scattering and for p-d quasi-elastic scattering are shown in the figure as well. The events distributed near the kinematical locus of p-d QES presumably correspond to p-(2N) reactions.

Now we summarize the results of present study for the backward proton emission mechanism. In Table IX we tabulate the various observed values, namely the slope factors (P_0) of the backward proton spectra ($\theta=118°$) and the power of A of the cross sections. We are led to the following conclusions:

(1) Forward-going particles in coincidence with backward protons ($350\leq P\leq 700$ MeV/c at 118°) are dominantly protons. The contribution of deuteron coincidences is about 10—20%. The contribution of coincident particles with mass number greater than 2 is very small.

(2) For the proton associated events, nucleon-nucleon quasi-free scattering gives only a small contribution to the backward inclusive cross section.

(3) The large in-plane to out-of-plane ratio indicates that backward protons are emitted mainly through a reaction in which only a few, most likely two or three, target nucleons are involved.

(4) The category "p-p non-QES" gives the largest contribution to backward proton production. The "p-p OPC" events also contribute significantly. However, the importance of "p-p OPC" decreases as the momentum of the backward proton increases because of the faster falloff of the spectrum (smaller P_0).

(5) The excess part of "p-p non-QES" events over "p-p OPC" events has a spectrum shape similar to that of "p-d QES." Therefore this part of the cross section is consistent with a reaction mechanism in which the incident proton scatters off a (2N) system inside the target nucleus.

It should be noted that the possibility of incoherent multiple scattering is in principle not rejected within the framework of the present data. Finally, if scattering from short range correlated clusters of three or more nucleons is important, effects should show up at angles larger than 15°. In the present experiment we also collected p-t events, but the statistics are too poor to isolate their contribution.

B. p-p quasi-elastic scatterings

We make a simple comparison of the "p-p QES" data to plane-wave impulse approximation (PWIA) calculations. Because the counter system did not have enough momentum resolution to separate the individual states of the residual nuclei, the component of "p-p QES" includes contributions from various final states. An effective internal momentum distribution was used instead of the momentum distribution obtained from the shell model wave functions. We assumed the momentum distribution to be a Gaussian,

$$F(P)dP^3=\exp(-P^2/2\sigma_p^2)dP^3\ , \tag{4.1}$$

where σ_p is 108.2 MeV/c, which corresponds to a Fermi momentum of 240 MeV/c. This momentum distribution is the one which has been successfully used to explain other p + nucleus data.[25,26] The binding energy of a proton is assumed to be 30 MeV.

The calculated shape of momentum spectrum of backward protons in coincidence with forward protons at $\theta=15°\pm4°$ agrees well with the spectrum of "p-p QES" (see Fig. 14). The angular distribution is also reproduced well by this model as shown by the dotted line in Fig. 16.

TABLE IX. Observations in pA collisions [θ_p(back) $=118°$].

		p + A → p + p + X			p + A → p + d + X			
	Inclusive	QES	non-QES	OPC	QES	non-QES	OPC	
Slope factor (P_0 in MeV/c)	87±2	55±5	91±6	68±6		94±8	73±7	$\frac{d^2\sigma}{dp\,d\Omega}\propto e^{-P/P_0}$, A=KCl, $\theta_1=15°$
Cross sections σ_I (in mb/rad sr)		0.05	0.80	0.47	0.03	0.16	0.11	very small dependence on A and angle A=KCl
Angular dependence		very sharp	slow	slow	sharp	slow	slow	A=KCl, independent of A
A dependence α in (A^α)	1.0	~0.55	~0.7	~0.8	~0.2	~0.7	~0.8	$\theta_1=15\sim40°$; A dependence is stronger for $\theta_1>70°$

C. p-d quasi-elastic scatterings and the properties of correlated clusters

In p-d quasi-elastic scattering, an incident proton is elastically scattered by a deuteronlike two-nucleon system (hereafter called "d") inside the target nucleus. The main reaction mechanism of p-d QES in present kinematical domain involves the pickup of a neutron from a "d" as shown in Fig. 22. This mechanism is also known to give the dominant contribution to the p-d elastic scatterings in the same kinematical domain.[27] Other possible mechanisms of p-d QES such as (a) double scattering of an incident proton with target nucleons followed by the coalescence of the scattered proton and neutron into deuteron, (b) p-p (or p-n) scattering followed by a neutron (or proton) pickup, (c) backscattering of an incident proton with a deuteron cluster, give small contributions.[28]

We now discuss the following questions: (1) how do the "d"'s move inside the nucleus? (2) what is the mean free path of deuterons inside the nucleus?

1. *Width of the sum-momentum (P_s) distribution*

The use of the plane wave impulse approximation (PWIA) should be appropriate in the present case, since distortions do not strongly affect the spectrum shape[29] but only the normalization. In PWIA the differential cross section [Σ(pd QES)] can be written as,

$$\Sigma(\text{pd QES}) = N_{\text{"d"}} D \int \Sigma(\text{pd el}) f(P_S) dP_S \ , \tag{4.2}$$

where $f(P_S)$ represents the momentum distribution of the "d" in the target nucleus, Σ(pd el) is the differential cross section of the p-d elastic scattering, $N_{\text{"d"}}$ is the total number of "d"'s inside the nucleus, and D is the attenuation factor due to the loss of particles along the path which the incident proton, the outgoing deuteron, and the outgoing proton traverse inside the target nucleus. The momentum distribution of the "d" inside the nucleus is assumed to be of the form $\exp(-P^2/2\sigma^2_{\text{"d"}})$. The width $\sigma_{\text{"d"}}$ as well as the binding energy of "d" to the nucleus BE("d") were taken as free parameters. The best fit to the data was obtained when $\sigma_{\text{"d"}} = 85 \pm 15$ MeV/c and BE("d") = 60 MeV. The momentum spectrum thus fitted is shown by the dashed curve in Fig. 23.

The present value of $\sigma_{\text{"d"}}$ is smaller than the momentum spread observed for deuteron fragments (as projectile fragments) in high-energy heavy-ion reactions, i.e., $\sigma_d = 135$ MeV/c for ^{12}C and ^{16}O projectiles at 2.1 GeV/nucleon of incident energy.[30,31] In what follows we discuss the cause of this difference. The root-mean-square (rms) momentum of the "d" can be written as,

$$\langle P_d^2 \rangle^{1/2} = (\langle P_p^2 \rangle + \langle P_n^2 \rangle + 2\langle P_p P_n \rangle)^{1/2} \ . \tag{4.3}$$

For a Gaussian distribution the rms value $\langle P^2 \rangle^{1/2}$ is related to the width σ by $\langle P^2 \rangle^{1/2} = \sqrt{3}\sigma$. Therefore,

$$\sigma_{\text{"d"}} = (\sigma_p^2 + \sigma_n^2 + \tfrac{2}{3}\langle P_p P_n \rangle)^{1/2} \ . \tag{4.4}$$

According to a purely statistical calculation,[32] the correlation term is given by

$$\langle P_p P_n \rangle = -\langle P_p^2 \rangle / (A-1) = -910 \ (\text{MeV}/c)^2 \ .$$

Here $\sigma_p = \sigma_n = 100$ MeV/c were used as obtained from the data of ep and pp quasi-elastic scatterings.[26,33] Then, Eq. (4.4) leads to $\sigma_d = 139$ MeV/c which is close to the value obtained in projectile fragmentation experiments ($\sigma_d = 135$ MeV/c). The much narrower width observed in p-d QES suggests that the "d," which is responsible for p-d QES, does not seem to originate from randomly selected two nucleons. Instead, it seems to originate from pn pairs which have a strong antiparallel momentum coupling ($\langle P_p P_n \rangle < 0$) since in this case the value of σ_d can be small. The fact that $\langle P_p P_n \rangle < 0$ may further indicate that high momentum protons originate from highly correlated nucleon pairs. The relation between σ_d and the two-particle momentum distribution was reported in Ref. 34.

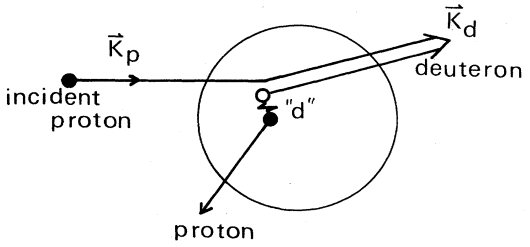

FIG. 22. The reaction mechanism for p-d QES at large momentum transfer. The incident proton picks up a neutron which has a momentum ($K_d - K_p$). The proton which was correlated with the neutron is emitted at a large angle.

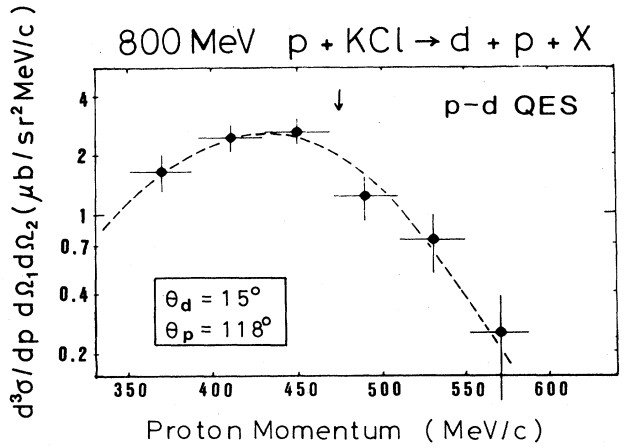

FIG. 23. Momentum spectra of backward protons associated with "p-d QES." The dashed curve shows the spectrum fitted to the data by a PWIA calculation. The momentum expected from p-d elastic scattering is indicated by the arrow.

2. *The mean free path of deuterons in nuclear matter*

Events that fall into the kinematical region of p-d QES are those in which the outgoing proton and deuteron are not rescattered inside the target nucleus after the first p-"d" collision. The attenuation of p-d QES depends on the mean free paths of the incident proton (λ_i), the back-

ward proton (λ_b), and the deuteron (λ_d). To estimate the attenuation factor D we perform a geometrical calculation similar to that used for p-p QES to obtain the mean free path of the proton inside the nucleus.[26] If we define the path length for the incident and the two outgoing particles by l_i, l_b, and l as shown in Fig. 24, then the attenuation factor (D) can be written as

$$D=\frac{\int e^{-l_i/\lambda_i}e^{-l_b/\lambda_b}e^{-l/\lambda_d}d\mathbf{r}}{\int d\mathbf{r}} . \tag{4.5}$$

The attenuation of p-p QES, which is measured at the same scattering angles, is obtained by Eq. (4.5) replacing λ_d by λ_p, the mean free path of the forward going proton. In general, the mean free paths depend on the particle energy. In the present discussion, however, only particles which have specific momenta, namely the momenta which satisfy the p-d or p-p QES, are discussed. Over this range of momenta the mean free paths are assumed to be energy independent. We assume further that the ratio of the probability of incident proton hitting a proton to that of hitting a "d" is constant inside the nucleus. The ratio (R) of the p-d QES to the p-p QES cross section then depends on the mass of the target only through λ_p and λ_d. The values of this ratio (R) obtained in the present experiment are plotted in Fig. 24. The abscissa of the figure is the mean path length $\langle l\rangle$ of the forward going particles defined as,

$$\langle l\rangle=\frac{\int e^{-l_i/\lambda_i}e^{-l_b/\lambda_b}l\,d\mathbf{r}}{\int e^{-l_i/\lambda_i}e^{-l_b/\lambda_b}d\mathbf{r}} . \tag{4.6}$$

The mean free paths of the incident and the backward protons are assumed to be $\lambda_i=2.5$ fm and $\lambda_b=5$ fm. Since the momentum range of backward protons was wide

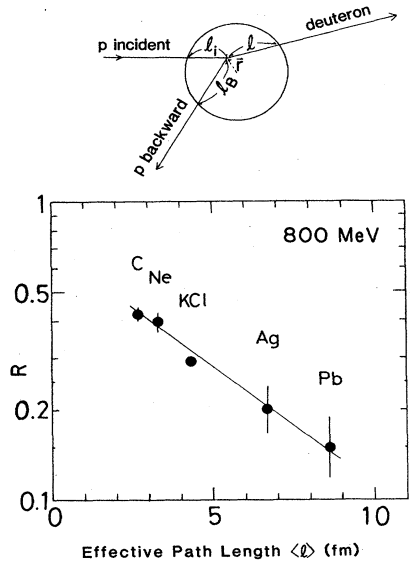

FIG. 24. The cross section ratio (R), σ(p-d QES)/σ(p-p QES), plotted as a function of the effective path length $\langle l\rangle$ of forward deuterons.

(330—550 MeV/c) the sensitivity of the result on λ_b was examined. The result was found to be insensitive to the value of λ_b over a wide range ($3\leq\lambda_b\leq 10$ fm).

The ratio (R) decreases sharply with increasing A, from which we conclude that deuterons (or "d"'s) are rescattered more frequently than protons as expected. The data were fitted by a function

$$\exp(-1/\lambda_d+1/\lambda_p)\langle l\rangle , \tag{4.7}$$

where λ_d and λ_p are the mean free paths of the deuteron in p-d QES and the forward going proton in p-p QES, respectively. Using the mean free path $\lambda_p=2.5$ fm,[26] λ_d is estimated to be 1.7 ± 0.3 fm at a deuteron momentum of 1.6 GeV/c. This mean free path is longer than the value $\lambda\approx 1.0$ fm which is calculated from d-p reaction cross section σ_r(dp) by

$$\lambda=\frac{1}{\rho\sigma_r(\mathrm{dp})} , \tag{4.8}$$

where $\rho=0.17$ fm^{-3} is the nucleon density of the nuclear matter.

V. CONCLUSIONS

We have measured the distribution of protons and deuterons associated with backward energetic protons over a wide kinematical range. The present experiment covers the kinematical region of both p-p and p-d quasi-elastic scatterings as well as quasi-deuteron breakups. We have demonstrated that various reaction mechanisms are kinematically separable. We have determined the slope factors of the backward proton spectra, the in-plane to out-of-plane ratios, the angular distributions, and the target mass dependences of the different components. Our data show that p-p quasi-elastic scatterings do not contribute much to the production of backward energetic protons. The process of "p-p non-QES" and "p-p OPC," which give the main contributions to backward energetic proton production, appear to be mainly from the proton scattering with a correlated nucleon cluster. The quantitative separation between cluster scattering and multiple scattering awaits further studies.

The data of p-d quasi-elastic scattering were analyzed with a plane wave impulse approximation. It is found that the momentum spread of the pn system ("d") inside the nucleus is smaller than that for deuterons observed in projectile fragments in high-energy heavy-ion collisions. The observed spread (85 ± 15 MeV/c) is also smaller than the width calculated from a purely statistical model. This result can be explained if it is assumed that the target "d," which is responsible for p-d QES, consists of a pn pair with an antiparallel momentum coupling between p and n which is stronger than expected from purely statistical consideration.

From the observed A dependence of the ratio between p-d QES to p-p QES cross sections, the mean free path of deuterons in the nucleus was estimated to be 1.7 ± 0.3 fm at $P_d=1.6$ GeV/c.

ACKNOWLEDGMENTS

The present measurements have been carried out at the Bevatron/Bevalac at the Lawrence Berkeley Laboratory. We acknowledge with thanks the important help by the Bevatron crews. Our special thanks go to R. Fuzesy for his technical support in the preparation of the experiment. Fruitful discussions with J. Knoll, J. Randrup, M. Sano, H. Sato, and H. Tezuka, are gratefully acknowledged. This work was supported by the Director, Division of Nuclear Physics of the Office of High Energy and Nuclear Physics of the U.S. Department of Energy under Contract DE-AC03-76SF00098, the Institute for Nuclear Study—Lawrence Berkeley Laboratory Collaboration Program, and by the U.S.—Japan Joint Program.

---

*Permanent address: Department of Physics, Faculty of Science, University of Tokyo, Hongo, Bunkyo-ku, Tokyo 113, Japan.

†Present address: Serin Physics Laboratory, Rutgers University, Piscataway, NJ 08854.

‡Also at Department of Physics, University of California, Berkeley, CA 94720.

[1]S. Frankel, W. Frati, O. Van Dyck, R. Werbeck, and V. Highland, Phys. Rev. Lett. **36**, 642 (1976).

[2]R. D. Amado and R. M. Woloshyn, Phys. Rev. Lett. **36**, 1435 (1976).

[3]S. Frankel, Phys. Rev. Lett. **38**, 1338 (1976).

[4]S. Frankel, Phys. Rev. C **17**, 694 (1978).

[5]S. Frankel, W. Frati, G. Blanpied, G. W. Hoffmann, T. Kozlowski, C. Morris, H. A. Thiessen, O. Van Dyck, R. Ridge, and C. Whitten, Phys. Rev. C **18**, 1375 (1978).

[6]S. Frankel, W. Frati, R. M. Woloshyn, and D. Yang, Phys. Rev. C **18**, 1378 (1978).

[7]C. F. Perdrisat, S. Frankel, and W. Frati, Phys. Rev. C **18**, 1764 (1978).

[8]Y. D. Bayukov, V. I. Efremenko, S. Frankel, W. Frati, M. Gazzaly, G. A. Leksin, N. A. Nikiforov, C. F. Perdrisat, V. I. Tchistilin, and Y. M. Zaitsev, Phys. Rev. C **20**, 764 (1979).

[9]S. Frankel, W. Frati, M. Gassaly, Y. D. Bayukov, V. I. Efremenko, G. A. Leskin, N. A. Nikiforov, V. I. Tchistilin, Y. M. Zaitsev, and C. F. Perdrisat, Phys. Rev. C **20**, 2257 (1979).

[10]S. A. Gurvitz, Phys. Rev. Lett. **47**, 560 (1981).

[11]T. Fujita, Phys. Rev. Lett. **39**, 174 (1977).

[12]T. Fujita and J. Hufner, Nucl. Phys **A314**, 317 (1979).

[13]T. Fujita, Nucl. Phys. **A324**, 409 (1979).

[14]T. Yukawa and S. Furui, Phys. Rev. C **20**, 2316 (1979).

[15]A. M. Baldin, in *High Energy Physics and Nuclear Structure—1975 (Santa Fe and Los Alamos)*, Proceedings of the Sixth International Conference on High Energy Physics and Nuclear Structure, AIP Conf. Proc. No. 26, edited by D. E. Nagle and A. S. Goldhaber (AIP, New York, 1975), p. 621, and references therein.

[16]J. Knoll, Phys. Rev. C **20**, 773 (1979).

[17]S. Frankel and R. M. Woloshyn, Phys. Rev. C **16**, 1680 (1977).

[18]S. Frankel, W. Frati, M. Gazzaly, G. W. Hoffmann, O. Van Dyck, and R. M. Woloshyn, Phys. Rev. Lett. **41**, 148 (1978); see also H. Brody, S. Frankel, W. Frati, and O. B. Van Dyck, Phys. Rev. C **24**, 2157 (1981).

[19]V. I. Komarov, G. E. Kosarev, H. Muller, D. Netzband, and T. Steihler, Phys. Lett. **69B**, 37 (1977).

[20]V. I. Komarov, G. E. Kosarev, H. Muller, D. Netzband, T. Stiehler, and S. Tesch, Phys. Lett. **80B**, 30 (1978).

[21]V. I. Komarov, G. E. Kosarev, H. Muller, D. Netzband, V. D. Toneev, T. Stiehler, S. Tesch, K. K. Gudima, and S. G. Mashnik, Nucl. Phys. **A326**, 297 (1979).

[22]S. Frankel, W. Frati, C. F. Perdrisat, and O. B. Van Dyck, Phys. Rev. C **24**, 2684 (1981).

[23]R. E. L. Green, D. H. Boal, R. Helmer, K. P. Jackson, and R. G. Korteling, Nucl. Phys. **A405**, 463 (1983).

[24]S. Nagamiya, M. C. Lemaire, E. Moeller, S. Schnetzer, G. Shapiro, H. Steiner, and I. Tanihata, Phys. Rev. C **24**, 971 (1981).

[25]J. Knoll and J. Randrup, Phys. Lett. **103B**, 264 (1981).

[26]I. Tanihata, S. Nagamiya, S. Schnetzer, and H. Steiner, Phys. Lett. **100B**, 121 (1981).

[27]G. Igo, Rev. Mod. Phys. **50**, 1 (1978).

[28]Y. Miake, Institute for Nuclear Study, University of Tokyo Report, INS-NUMA-39, 1982.

[29]D. F. Jackson and B. K. Jain, Phys. Lett. **27B**, 147 (1968).

[30]D. E. Greiner, P. J. Lindstrom, H. H. Heckmann, B. Cork, and F. S. Bieser, Phys. Rev. Lett. **35**, 152 (1974).

[31]L. Anderson, W. Bruckner, E. Moeller, S. Nagamiya, S. Nissen-Meyer, L. Schroeder, G. Shapiro, and H. Steiner, Phys. Rev. C **28**, 1224 (1983).

[32]A. S. Goldhaber, Phys. Lett. **53B**, 306 (1974).

[33]E. J. Moniz, I. Sick, R. R. Whitney, J. R. Ficenec, R. D. Kephart, and W. P. Trower, Phys. Rev. Lett. **26**, 445 (1971).

[34]I. Tanihata, in Proceedings of the 1983 Institute for Nuclear Study International Symposium on High Energy Photo-Nuclear Reactions and Related Topics, edited by S. Homma, Tokyo, Japan, p. 215.